Chapter 3
Are Rotational DoFs Essential in Substructure Decoupling?

Walter D'Ambrogio and Annalisa Fregolent

Abstract Substructure decoupling consists in the identification of the dynamic behavior of a structural subsystem, starting from the known dynamic behavior of both the coupled system and the remaining part of the structural system (residual subsystem). The degrees of freedom (DoFs) of the coupled system can be partitioned into internal DoFs (not belonging to the couplings) and coupling DoFs. In direct decoupling, a fictitious subsystem that is the negative of the residual subsystem is added to the coupled system, and appropriate compatibility and equilibrium conditions are enforced at interface DoFs. Compatibility and equilibrium can be required either at coupling DoFs only (standard interface), or at additional internal DoFs of the residual subsystem (extended interface), or at some coupling DoFs and/or some internal DoFs of the residual subsystem (mixed interface). Using a mixed interface, rotational coupling DoFs could be eliminated and substituted by internal translational DoFs. This would avoid difficult measurements of rotational FRFs. This possibility is verified in this paper using simulated experimental data.

Keywords Substructure decoupling • Rotational DoFs • Mixed interface • Experimental dynamic substructuring • Frequency based substructuring

3.1 Introduction

The identification of the dynamic behaviour of a structural subsystem, starting from the known dynamic behaviour of both the coupled system and the remaining part of the structural system (residual subsystem), is also known as decoupling problem, subsystem subtraction or inverse dynamic substructuring. Decoupling is a relevant issue for subsystems that cannot be tested separately, but only when coupled to their neighboring substructure(s) (e.g. a fixture needed for testing or subsystems in operational conditions).

Decoupling is a special case of experimental dynamic substructuring, where experimental means that the model of at least one subsystem derives from tests. In Frequency Based Substructuring, Frequency Response Functions (FRFs) are used instead of modal parameters. A general framework for dynamic substructuring is provided in [1], where the primal assembly and the dual assembly are introduced.

Decoupling is a very critical problem even in apparently trivial applications. It has been highlighted that subsystem identification problems are affected by ill-conditioning around a discrete number of frequencies, that depends on the choice of the measured DoFs [2, 3]. Additional problems arise that are strictly connected with the use of measured FRFs: among others, systematic errors and inconsistencies.

Furthermore, a well known issue in experimental dynamic substructuring is related to rotational DoFs. In substructure coupling, whenever coupling DoFs include rotational DoFs, the related rotational FRFs must be obtained experimentally.

W. D'Ambrogio (✉)
Dipartimento di Ingegneria Industriale e dell'Informazione e di Economia, Università dell'Aquila, Via G. Gronchi, 18
I-67100, L'Aquila (AQ), Italy
e-mail: walter.dambrogio@univaq.it

A. Fregolent
Dipartimento di Ingegneria Meccanica e Aerospaziale, Università di Roma La Sapienza, Via Eudossiana 18, I 00184 Rome, Italy
e-mail: annalisa.fregolent@uniroma1.it

M. Allen et al. (eds.), *Dynamics of Coupled Structures, Volume 1: Proceedings of the 32nd IMAC, A Conference and Exposition on Structural Dynamics, 2014*, Conference Proceedings of the Society for Experimental Mechanics Series,
DOI 10.1007/978-3-319-04501-6_3, © The Society for Experimental Mechanics, Inc. 2014

This becomes a quite complicated task when measuring only translational FRFs, as shown in [4]. Several techniques for measuring rotational responses have been devised since then, see e.g. [5, 6]. However, when such rotational FRFs are used for substructure coupling, results are still unsatisfactory.

For some time, it was believed that issues related to rotational DoFs also applied to substructure decoupling. However, in this case the effect of rotational DoFs is already embedded in each measured FRF of the assembled system, whose dynamics depends on how subsystems are connected together. In practice, the use of a mixed interface [7] may allow to substitute some unwanted connecting DoFs with internal DoFs of the residual substructure: unwanted connecting DoFs include rotational DoFs and DoFs that should for instance be measured at bolted joints.

In this paper, it is attempted to answer a question on how essential are rotational DoFs in substructure decoupling. To this aim, simulated test data on a fixed–fixed beam made by two cantilever beams joined together, are used.

3.2 Direct Decoupling Techniques

The coupled structural system RU (N_{RU} DoFs) is assumed to be made by an unknown subsystem U (N_U DoFs) and a residual subsystem R (N_R DoFs) joined through a number of couplings (see Fig. 3.1). The degrees of freedom (DoFs) of the coupled system can be partitioned into internal DoFs (not belonging to the couplings) of subsystem U (u), internal DoFs of subsystem R (r), and coupling DoFs (c).

It is required to find the FRF of the unknown substructure U starting from the FRFs of the coupled system RU and of the residual subsystem R. The subsystem U can be extracted from the coupled system RU by cancelling the dynamic effect of the residual subsystem R. This can be accomplished by adding to the coupled system RU a "negative" subsystem with a dynamic stiffness opposite to that of the residual subsystem R. The dynamic equilibrium of the coupled system RU and of the negative subsystem is expressed in block diagonal format as:

$$\begin{bmatrix} \mathbf{Z}^{\mathbf{RU}} & \mathbf{0} \\ \mathbf{0} & -\mathbf{Z}^{\mathbf{R}} \end{bmatrix} \begin{Bmatrix} \mathbf{u}^{\mathbf{RU}} \\ \mathbf{u}^{\mathbf{R}} \end{Bmatrix} = \begin{Bmatrix} \mathbf{f}^{\mathbf{RU}} \\ \mathbf{f}^{\mathbf{R}} \end{Bmatrix} + \begin{Bmatrix} \mathbf{g}^{\mathbf{RU}} \\ \mathbf{g}^{\mathbf{R}} \end{Bmatrix} \tag{3.1}$$

where:

- $\mathbf{Z}^{\mathbf{RU}}$, $\mathbf{Z}^{\mathbf{R}}$ are the dynamic stiffness matrices of the coupled system RU and of the residual subsystem R;
- $\mathbf{u}^{\mathbf{RU}}$, $\mathbf{u}^{\mathbf{R}}$ are the vectors of degrees of freedom of the coupled system RU and of the residual subsystem R;
- $\mathbf{f}^{\mathbf{RU}}$, $\mathbf{f}^{\mathbf{R}}$ are the external force vectors on the coupled system RU and on the fictitious subsystem;
- $\mathbf{g}^{\mathbf{RU}}$, $\mathbf{g}^{\mathbf{R}}$ are the vectors of connecting forces between the coupled system and the fictitious subsystem, and viceversa (constraint forces associated with compatibility conditions).

According to this point of view, the interface between the coupled system RU and the fictitious subsystem should not only include all the coupling DoFs between subsystems U and R, but should as well include all the internal DoFs of subsystem R. However, it can be shown that the problem can be solved by considering a number of interface DoFs at least equal to the number of coupling DoFs n_c. Therefore, three options for interface DoFs can be considered:

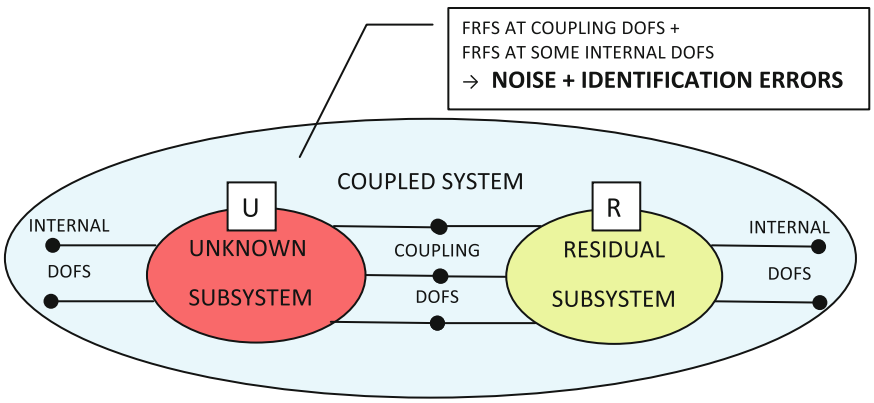

Fig. 3.1 Scheme of the decoupling problem

- standard interface, including only the coupling DoFs (c) between subsystems U and R;
- extended interface, including the coupling DoFs and a subset of internal DoFs ($i \subseteq r$) subsystem R;
- mixed interface, including subsets of coupling DoFs ($d \subseteq c$) and/or internal DoFs ($i \subseteq r$) of subsystem R.

The use of a mixed interface may allow to substitute rotational coupling DoFs with translational internal DoFs.

The compatibility condition at the (standard, extended, mixed) interface DoFs implies that any pair of matching DoFs u_l^{RU} and u_m^R, i.e. DoF l on the coupled system RU and DoF m on subsystem R must have the same displacement, that is $u_l^{RU} - u_m^R = 0$. Let the number of interface DoFs on which compatibility is enforced be denoted as N_C.

The compatibility condition can be generally expressed as:

$$\left[\mathbf{B}_\mathbf{C}^\mathbf{RU}\ \mathbf{B}_\mathbf{C}^\mathbf{R}\right]\left\{\begin{matrix}\mathbf{u}^\mathbf{RU}\\ \mathbf{u}^\mathbf{R}\end{matrix}\right\} = \mathbf{0} \tag{3.2}$$

where each row of $\mathbf{B_C} = \left[\mathbf{B}_\mathbf{C}^\mathbf{RU}\,\mathbf{B}_\mathbf{C}^\mathbf{R}\right]$ corresponds to a pair of matching DoFs. Note that $\mathbf{B_C}$ has size $N_C \times (N_{RU} + N_R)$ and is, in most cases, a signed Boolean matrix.

It should be noted that the interface DoFs involved in the equilibrium condition need not to be the same as DoFs used to enforce compatibility. In this case, the approach is called non-collocated [7], whereas the traditional approach, in which compatibility and equilibrium DoFs are the same, is called collocated.

Let N_E denote the number of interface DoFs on which equilibrium is enforced. The equilibrium of constraint forces implies that their sum must be zero for any pair of matching DoFs, i.e. $g_r^{RU} + g_s^R = 0$. Furthermore, for any DoF k not involved in the equilibrium condition, it must be $g_k^{RU} = 0$ and $g_k^R = 0$.

Overall, the above conditions can be expressed as:

$$\left[\begin{matrix}\mathbf{L}_\mathbf{E}^\mathbf{RU}\\ \mathbf{L}_\mathbf{E}^\mathbf{R}\end{matrix}\right]^T\left\{\begin{matrix}\mathbf{g}^\mathbf{RU}\\ \mathbf{g}^\mathbf{R}\end{matrix}\right\} = \mathbf{0} \tag{3.3}$$

where the matrix $\mathbf{L_E} = \left[\mathbf{L}_\mathbf{E}^\mathbf{RU}\,\mathbf{L}_\mathbf{E}^\mathbf{R}\right]$ is a Boolean localisation matrix. Note that the number of columns of $\mathbf{L_E}$ is equal to the number N_E of equilibrium interface DoFs plus the number N_{NE} of DoFs not belonging to the equilibrium interface. Note that $N_{NE} = N_{RU} + N_R - 2N_E$: in fact, the number of DoFs belonging to the equilibrium interface must be subtracted once from N_{RU} and once from N_R. Therefore, the size of $\mathbf{L_E}$ is $(N_{RU} + N_R) \times (N_{RU} + N_R - N_E)$.

Equations (3.1)–(3.3) can be gathered to obtain the so-called three-field formulation. Starting from the three-field formulation, several assembly techniques can be devised:

- dual assembly [1, 3] where equilibrium is satisfied exactly by defining a unique set of connecting force intensities;
- primal assembly [1, 8] where compatibility is satisfied exactly by defining a unique set of interface DoFs;
- hybrid assembly [9] where both compatibility and equilibrium are satisfied exactly.

In the sequel, only the dual assembly is recalled. It can be shown [9] that whenever $N_C = N_E$, i.e. the number of compatibility DoFs is the same as the number of equilibrium DoFs, all assembly techniques provide the same result.

3.2.1 Dual Assembly

In the dual assembly, the equilibrium condition $g_r^{RU} + g_s^R = 0$ at a pair of equilibrium interface DoFs is ensured by choosing $g_r^{RU} = -\lambda$ and $g_s^R = \lambda$. If a Boolean matrix $\mathbf{B_E}$ related to interface equilibrium DoFs is defined similarly to $\mathbf{B_C}$, the overall interface equilibrium can be ensured by writing the connecting forces in the form:

$$\left\{\begin{matrix}\mathbf{g}^\mathbf{RU}\\ \mathbf{g}^\mathbf{R}\end{matrix}\right\} = -\left[\begin{matrix}\mathbf{B}_\mathbf{E}^{\mathbf{RU}\,T}\\ \mathbf{B}_\mathbf{E}^{\mathbf{R}\,T}\end{matrix}\right]\boldsymbol{\lambda} \tag{3.4}$$

where $\boldsymbol{\lambda}$ are Lagrange multipliers corresponding to connecting force intensities and $\mathbf{B_E}$ is a $N_E \times (N_{RU} + N_R)$ matrix. Since there is a unique set of connecting force intensities $\boldsymbol{\lambda}$, the interface equilibrium condition is satisfied automatically for any $\boldsymbol{\lambda}$, i.e.

$$\begin{bmatrix} \mathbf{L_E^{RU}} \\ \mathbf{L_E^{R}} \end{bmatrix}^T \begin{Bmatrix} \mathbf{g^{RU}} \\ \mathbf{g^{R}} \end{Bmatrix} = - \begin{bmatrix} \mathbf{L_E^{RU}} \\ \mathbf{L_E^{R}} \end{bmatrix}^T \begin{bmatrix} \mathbf{B_E^{RU}}^T \\ \mathbf{B_E^{R}}^T \end{bmatrix} \boldsymbol{\lambda} = \mathbf{0} \tag{3.5}$$

In the dual assembly, the total set of DoFs is retained, i.e. each interface DoF appears twice. Since Eq. (3.5) is always satisfied, the three-field formulation reduces to:

$$\begin{cases} \begin{bmatrix} \mathbf{Z^{RU}} & \mathbf{0} \\ \mathbf{0} & -\mathbf{Z^{R}} \end{bmatrix} \begin{Bmatrix} \mathbf{u^{RU}} \\ \mathbf{u^{R}} \end{Bmatrix} + \begin{bmatrix} \mathbf{B_E^{RU}}^T \\ \mathbf{B_E^{R}}^T \end{bmatrix} \boldsymbol{\lambda} = \begin{Bmatrix} \mathbf{f^{RU}} \\ \mathbf{f^{R}} \end{Bmatrix} & (3.1^*) \\ \begin{bmatrix} \mathbf{B_C^{RU}} & \mathbf{B_C^{R}} \end{bmatrix} \begin{Bmatrix} \mathbf{u^{RU}} \\ \mathbf{u^{R}} \end{Bmatrix} = \mathbf{0} & (3.2) \end{cases}$$

or in more compact form:

$$\begin{cases} \mathbf{Z}\mathbf{u} + \mathbf{B_E}^T \boldsymbol{\lambda} = \mathbf{f} & (3.1^*) \\ \mathbf{B_C}\mathbf{u} = \mathbf{0} & (3.2) \end{cases}$$

To eliminate $\boldsymbol{\lambda}$, Eq. (3.1*) can be written:

$$\mathbf{u} = -\mathbf{Z}^{-1}\mathbf{B_E}^T \boldsymbol{\lambda} + \mathbf{Z}^{-1}\mathbf{f} \tag{3.1*}$$

which substituted in Eq. (3.2) gives:

$$\mathbf{B_C}\mathbf{Z}^{-1}\mathbf{B_E}^T \boldsymbol{\lambda} = \mathbf{B_C}\mathbf{Z}^{-1}\mathbf{f} \tag{3.6}$$

from which $\boldsymbol{\lambda}$, to be back-substituted in Eq. (3.1*), is found as:

$$\boldsymbol{\lambda} = \left(\mathbf{B_C}\mathbf{Z}^{-1}\mathbf{B_E}^T\right)^+ \mathbf{B_C}\mathbf{Z}^{-1}\mathbf{f} \tag{3.7}$$

To obtain a determined or overdetermined matrix for the generalized inversion operation, the number of rows of $\mathbf{B_C}$ must be greater or equal than the number of rows of $\mathbf{B_E}$, i.e.

$$N_C \geq N_E \geq n_c \tag{3.8}$$

Note that, if $N_C > N_E$, Eq. (3.6) is not satisfied exactly by vector $\boldsymbol{\lambda}$ given by Eq. (3.7), but only in the minimum square sense. This implies that also Eq. (3.2) is not satisfied exactly, i.e. compatibility conditions at interface are approximately satisfied. On the contrary, equilibrium is satisfied exactly due to the introduction of the connecting force intensities $\boldsymbol{\lambda}$ as in Eq. (3.4).

By substituting $\boldsymbol{\lambda}$ in Eq. (3.1*), it is obtained:

$$\mathbf{Z}\mathbf{u} + \mathbf{B_E}^T \left(\mathbf{B_C}\mathbf{Z}^{-1}\mathbf{B_E}^T\right)^+ \mathbf{B_C}\mathbf{Z}^{-1}\mathbf{f} = \mathbf{f} \tag{3.9}$$

Finally, $\mathbf{u}$ can be written as $\mathbf{u} = \mathbf{H}\mathbf{f}$, which provides the FRF of the unknown subsystem U:

$$\mathbf{u} = \left(\mathbf{Z}^{-1} - \mathbf{Z}^{-1}\mathbf{B_E}^T \left(\mathbf{B_C}\mathbf{Z}^{-1}\mathbf{B_E}^T\right)^+ \mathbf{B_C}\mathbf{Z}^{-1}\right)\mathbf{f} \tag{3.10}$$

i.e., by noting that the inverse of the block diagonal dynamic stiffness matrix can be expressed as:

$$\begin{bmatrix} \mathbf{Z^{RU}} & \mathbf{0} \\ \mathbf{0} & -\mathbf{Z^{R}} \end{bmatrix} = \mathbf{Z}^{-1} = \mathbf{H} = \begin{bmatrix} \mathbf{H^{RU}} & \mathbf{0} \\ \mathbf{0} & -\mathbf{H^{R}} \end{bmatrix} \tag{3.11}$$

where $\mathbf{H^{RU}}$ and $\mathbf{H^{R}}$ are the FRFs of the assembled structure and of the residual substructure, it is:

$$\mathbf{H}^{\mathbf{U}} = \mathbf{H} - \mathbf{H}\mathbf{B}_{\mathbf{E}}{}^{T} \left(\mathbf{B}_{\mathbf{C}}\mathbf{H}\mathbf{B}_{\mathbf{E}}{}^{T}\right)^{+} \mathbf{B}_{\mathbf{C}}\mathbf{H} \tag{3.12}$$

With the dual assembly, the rows and the columns of $\mathbf{H}^{\mathbf{U}}$ corresponding to compatibility and equilibrium DoFs appear twice. Furthermore, when using an extended or mixed interface, $\mathbf{H}^{\mathbf{U}}$ contains some meaningless rows and columns: those corresponding to the internal DoFs of the residual substructure R. Obviously, only meaningful and independent entries are retained.

3.3 Test Structure

The proposed decoupling technique is tested on an aluminium beam (Fig. 3.2). The residual substructure R (left) consists of a long uniform cantilever beam (1). The unknown substructure U (right) is a short uniform cantilever beam (2). The two substructures are assumed to be rigidly connected at the free ends, involving both translational and rotational DoFs.

The mechanical properties of the structures are: $E = 7.0 \cdot 10^{10}\,\mathrm{N/m^2}$, $\rho = 2{,}700\,\mathrm{kg/m^3}$, modal damping $\zeta = 0.005$. The geometrical properties of the items are shown in Table 3.1.

To verify the limits and the reliability of the decoupling technique, an analysis is performed using simulated data, eventually polluted by random noise. An FE model of both substructures is built using beam elements. The FE model of the assembled structure is obtained by assembling the FE models of the two substructures. Inertance FRFs are obtained from the FE models at DoFs shown in Fig. 3.2: among them, DoFs $9y$ and $9\vartheta_z$ are the coupling DoFs, DoFs $1y$–$8y$ are internal DoFs of the residual substructure R, and DoFs $10y$–$13y$ are internal DoF of the unknown substructure U. Table 3.2 shows the natural frequencies of the two substructures and of the assembled structure, obtained from FE models.

To simulate the effect of noise on the FRFs of the assembled structure and of the residual substructure, a complex random perturbation is added to FRFs $\hat{H}_{rs}$ computed from the FE model:

$$H_{rs}(\omega_k) = \hat{H}_{rs}(\omega_k) + m_{rs,k} + i\, n_{rs,k} \tag{3.13}$$

where $m_{rs,k}$ and $n_{rs,k}$ are independent random variables with gaussian distribution, zero mean and a standard deviation proportional to the average value of the FRF modulus.

3.4 Decoupling

The FRFs of subsystem U can be determined by using the procedure described previously and summarized in Eq. (3.12), where compatibility and equilibrium DoFs are defined case by case.

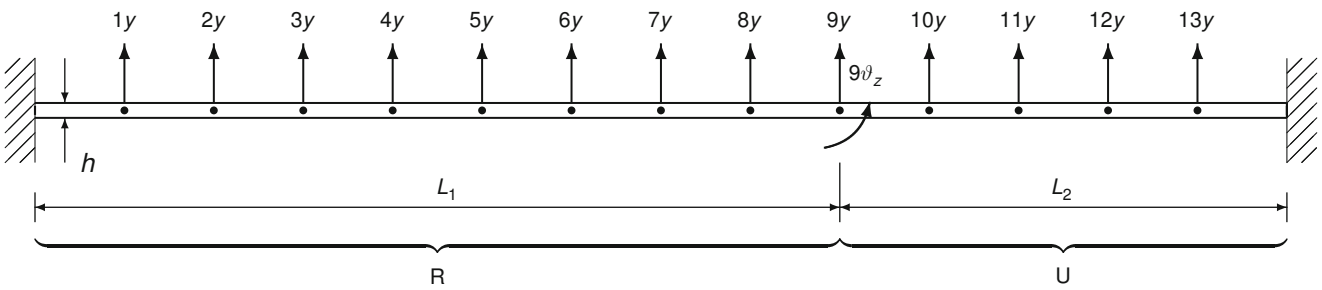

Fig. 3.2 Sketch of the test structure

Table 3.1 Geometrical dimensions

Item	Length (mm)	Width (mm)	Height (mm)
1. Long beam	540	40	8
2. Short beam	300	40	8

Table 3.2 Natural frequencies

Mode	1	2	3	4	5
Assembled structure RU	59.34	163.58	320.68	530.09	791.87
Residual substructure R	22.57	141.42	395.97	775.95	–
Unknown substructure U	73.11	458.19	–	–	–

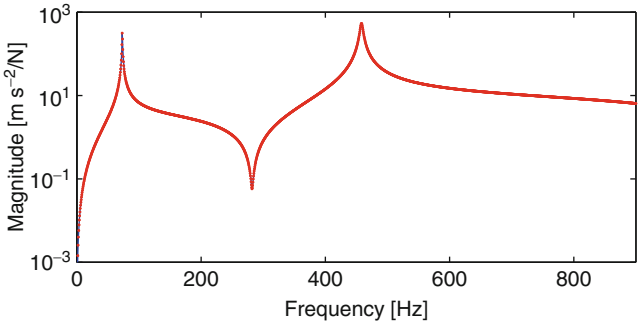

Fig. 3.3 $H^{U}_{11y,11y}$: true (—), computed using either standard interface with coupling DoFs $9y$, $9\vartheta_z$ (⁎⁎⁎), or mixed interface with internal DoFs $1y$, $5y$, $8y$ (⁎⁎⁎) (Color figure online)

3.4.1 Results Without Added Noise

First of all, the case of standard interface (FRFs known only at the coupling DoFs $9y$ and $9\vartheta_z$) is considered. The internal DoF $11y$ of the unknown substructure U is used as a reference DoF to compare results obtained even when no coupling DoF is included among interface DoFs. In this case, $N_C = 2$, $N_E = 2$, $N_O = 1$ and

$$\mathbf{B_C} = \mathbf{B_E} = \begin{array}{c} \begin{matrix} u^{RU}_{9y} & u^{RU}_{9\vartheta_z} & u^{RU}_{11y} & u^{R}_{9y} & u^{R}_{9\vartheta_z} \end{matrix} \\ \left[\begin{array}{ccc|cc} 1 & 0 & 0 & -1 & 0 \\ 0 & 1 & 0 & 0 & -1 \end{array}\right] \\ \mathbf{B^{RU}_C} \qquad\qquad \mathbf{B^{R}_C} \end{array} \tag{3.14}$$

As expected, the FRF of the unknown subsystem is predicted without errors (Fig. 3.3).

Since the coupling DoFs can be difficult to measure, especially when, as in the present case, they include rotational DoFs, a mixed interface is considered that uses only internal DoFs $1y$, $5y$, $8y$. Again, the internal DoF $11y$ of the unknown substructure U is used as a reference DoF. Therefore $N_C = 3$, $N_E = 3$, $N_O = 1$ and

$$\mathbf{B_C} = \mathbf{B_E} = \begin{array}{c} \begin{matrix} u^{RU}_{1y} & u^{RU}_{5y} & u^{RU}_{8y} & u^{RU}_{11y} & u^{R}_{1y} & u^{R}_{5y} & u^{R}_{8y} \end{matrix} \\ \left[\begin{array}{cccc|ccc} 1 & 0 & 0 & 0 & -1 & 0 & 0 \\ 0 & 1 & 0 & 0 & 0 & -1 & 0 \\ 0 & 0 & 1 & 0 & 0 & 0 & -1 \end{array}\right] \\ \mathbf{B^{RU}_C} \qquad\qquad\qquad\qquad \mathbf{B^{R}_C} \end{array} \tag{3.15}$$

Also in this case, the FRF of the unknown substructure U is predicted without errors: in Fig. 3.3 the predicted FRF is hidden by the FRF obtained using the standard interface. Although this result could be expected from theory, nevertheless it seems quite surprising that the FRF of the unknown substructure can be obtained without considering the FRFs at the coupling DoFs.

3.4.2 Results Using Raw FRFs with Added Noise of 0.05 %

This step is aimed to highlight ill-conditioning problems and other possible troubles that might arise due to the choice of interface DoFs. A very small amount of noise, i.e. 0.05 % of the average value of each FRF, is enough to trigger such effects. Furthermore, the use of raw FRFs avoids fitting error and its influence.

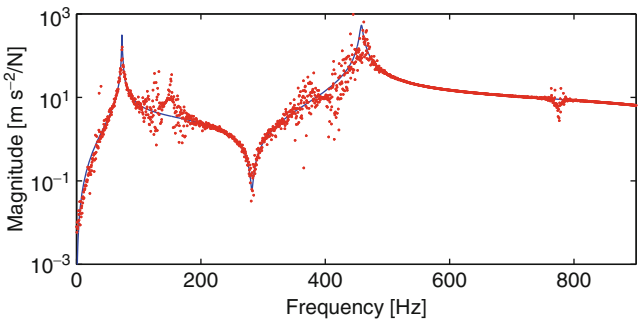

Fig. 3.4 $H^{U}_{11y,11y}$: true (—), computed using standard interface with coupling DoFs $9y$, $9\vartheta_z$ (∗∗∗) (Color figure online)

Table 3.3 Natural frequencies of subsystem R with interface DoFs locked, below 900 Hz

Interface DoFs	Ill-conditioned frequencies		
$9y$, $9\vartheta_z$	143.6	395.8	776.0
$9y$, $9\vartheta_z$, $1y$	172.2	476.9	–
$1y$, $5y$, $8y$	474.5	683.0	–

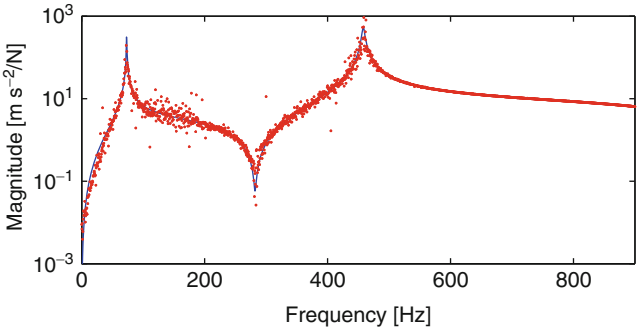

Fig. 3.5 $H^{U}_{11y,11y}$: true (—), computed using extended interface with coupling DoFs $9y$, $9\vartheta_z$ and additional internal DoF 1 $(1, 0.00, 0.00{*}{*}{*})$ (Color figure online)

The case of standard interface (FRFs known only at the coupling DoFs $9y$, $9\vartheta_z$ and at the internal DoF $11y$ of the unknown substructure U) is considered first. The matrix $\mathbf{B_C} = \mathbf{B_E}$ is still given by Eq. (3.14). The predicted FRF of the unknown substructure U is shown in Fig. 3.4: it can be noticed that the peak around the second natural frequency presents some scatter, and some spurious peaks due to ill conditioning appear at frequencies 143.6, 395.8 and 776 Hz as reported in the first row of Table 3.3. As shown in [3], such frequencies are the natural frequencies of the residual subsystem with interface DoFs locked.

Normally, results are improved by using an extended interface that involves, together with coupling DoFs, some additional internal DoFs of the residual substructure. Therefore, besides the coupling DoFs $9y$, $9\vartheta_z$, the additional internal DoF $1y$ is used. Again, the internal DoF $11y$ of the unknown substructure U is used as a reference DoF. Therefore $N_C = 3$, $N_E = 3$, $N_O = 1$ and

$$\mathbf{B_C} = \mathbf{B_E} = \begin{array}{c} \begin{matrix} u^{RU}_{9y} & u^{RU}_{9\vartheta_z} & u^{RU}_{1y} & u^{RU}_{11y} & u^{R}_{9y} & u^{R}_{9\vartheta_z} & u^{R}_{1y} \end{matrix} \\ \left[\begin{array}{cccc|ccc} 1 & 0 & 0 & 0 & -1 & 0 & 0 \\ 0 & 1 & 0 & 0 & 0 & -1 & 0 \\ 0 & 0 & 1 & 0 & 0 & 0 & -1 \end{array}\right] \\ \mathbf{B^{RU}_C} \qquad\qquad \mathbf{B^{R}_C} \end{array} \tag{3.16}$$

The predicted FRF of the unknown substructure U is shown in Fig. 3.5: the peak around the second natural frequency is better defined, and some scatter appears around the ill conditioned frequency of 172 Hz (see second row of Table 3.3). As expected, there is some definite improvement with respect to the standard interface. Also, it can be noticed that the effect of the ill conditioned frequency around 477 Hz can be masked by the resonance at the close frequency of 458 Hz.

To avoid using coupling DoFs, a mixed interface is again considered, including only internal DoFs $1y$, $5y$, $8y$, and the internal DoF $11y$ of the unknown substructure U. The matrix $\mathbf{B_C} = \mathbf{B_E}$ is still given by Eq. (3.15). The predicted FRF of the unknown substructure U is shown in Fig. 3.6: some scatter appears around the antiresonance and the second natural frequency, and, quite surprisingly, the overall FRF is improved with respect to the one obtained using standard interface. Both the ill conditioned frequencies (see third row of Table 3.3) seem to have no effect.

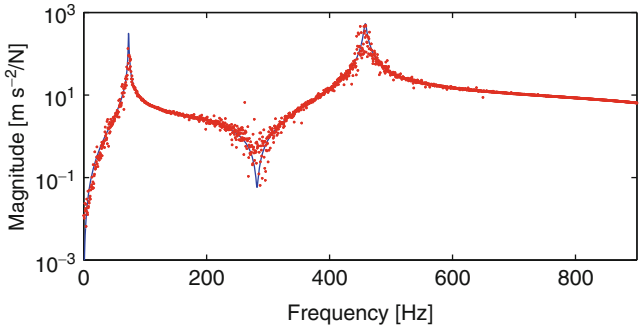

Fig. 3.6 $H^U_{11y,11y}$: true (—), computed using mixed interface with internal DoFs $1y$, $5y$, $8y$ (∗∗∗) (Color figure online)

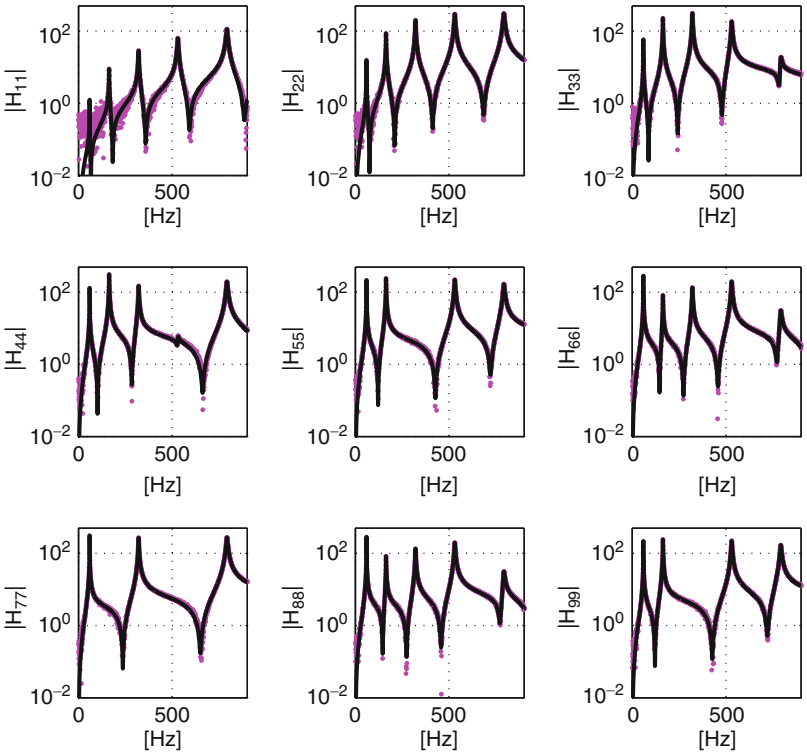

Fig. 3.7 Noise polluted (∗∗∗), and fitted (—) drive point FRFs of the coupled structure (Color figure online)

3.4.3 Results Using Fitted FRFs with Added Noise of 1 %

A more realistic noise level of 1 % of the average value of each FRF in the frequency range 0–2,000 Hz is used. In this case, raw FRFs are unable to provide any result. Therefore, the FRFs are curve fitted using a polyreference least square complex frequency domain technique having assumed that only translational FRFs are available. Figure 3.7 shows the raw (noise polluted) and fitted drive point FRFs of the coupled structure RU. Similar results are obtained for the residual substructure R.

In this case, the rotational coupling DoF $9\theta_z$ is not available. Therefore, the use of standard and extended interfaces is not permitted.

First, the largest possible mixed interface is used, including the translational coupling DoFs $9y$ and all the internal DoFs $1y$–$8y$, so that $N_C = 9$, $N_E = 9$, $N_O = 1$ and the matrix expressing the compatibility condition is built accordingly. The predicted FRF of the unknown substructure U is shown in Fig. 3.8: although the predicted FRFs is quite clean, some shifts of the natural frequencies and of the antiresonance appear. Moreover, the dynamic range is significantly reduced.

In practice, it can be complicated to measure such a large number of internal DoFs. Therefore, some attempts are performed using a limited number of internal DoFs. One of the best result is obtained using a mixed interface with coupling DoF $9y$ and internal DoFs $1y$, $3y$, $5y$. In this case, $N_C = 4$, $N_E = 4$, $N_O = 1$ and the matrix expressing the compatibility condition is built accordingly. The predicted FRF of the unknown substructure U is shown in Fig. 3.9: the predicted FRFs is quite clean, as usual when using fitted FRFs. However, larger shifts of the natural frequencies and of the antiresonance appear together with a significant reduction of the dynamic range.

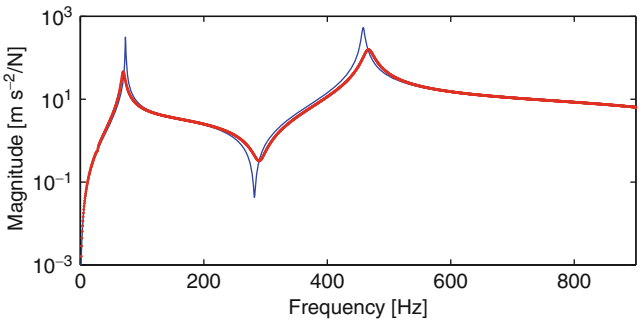

Fig. 3.8 $H^U_{11,11}$: true (—), computed from fitted FRFs using mixed interface with coupling DoF $9y$ and internal DoFs $1y$–$8y$ (∗∗∗) (Color figure online)

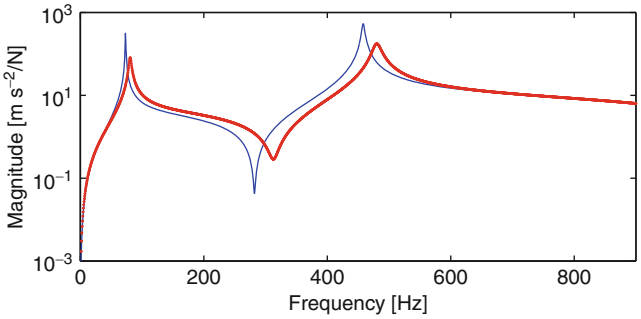

Fig. 3.9 $H^U_{11,11}$: true (—), computed from fitted FRFs using mixed interface with coupling DoF $9y$ and internal DoFs $1y$, $3y$, $5y$ (∗∗∗) (Color figure online)

In both the reported cases, and to a larger extent when different sets of internal DoFs are used, it seems that the systematic error due to the curve fitting procedure significantly affects the precision of the predicted FRFs and especially the location of resonances and antiresonances, and the sharpness of the related peaks and dips.

3.5 Summary and Discussion

In this paper, it is tried to establish if rotational DoFs, possibly included among the connecting DoFs, are essential in substructure decoupling. In fact, the experimental estimation of rotational FRFs is a quite complicated task.

Differently from the coupling problem, where rotational DoFs can not be neglected, in the decoupling case this is possible because the actions exchanged through the connecting DoFs, and specifically through rotational DoFs, are already embedded in each FRF of the assembled system. In the decoupling case, a mixed interface can in fact be considered that allows to substitute undesired coupling DoFs with internal DoFs of the residual subsystem.

To check the procedure, simulated test data on a fixed–fixed beam made by two cantilever beams joined together, are used. Using FRFs without added noise, the FRFs of the unknown substructure are correctly predicted, both using a standard interface including only coupling DoFs and using a mixed interface without coupling DoFs. By considering raw FRFs with added noise, the results obtained using a mixed interface without coupling DoFs are much less scattered than those obtained using a standard interface and not worse than the results obtained using an extended interface. By considering FRFs fitted after adding noise, the results using a mixed interface without the rotational DoF show some resonance and antiresonance shifts, and a significant reduction of the dynamic range. Both effects could be ascribed to systematic errors on FRFs due to the curve fitting procedure.

According to the obtained results, it can be stated that, as predicted by the theory, rotational DoFs are not essential in the decoupling problem. They can be substituted by internal translational DoFs without altering the results.

Acknowledgements This research is supported by grants from University of Rome La Sapienza and University of L'Aquila.

References

1. de Klerk D, Rixen DJ, Voormeeren S (2008) General framework for dynamic substructuring: history, review, and classification of techniques. AIAA J 46(5):1169–1181
2. Sjövall P, Abrahamsson T (2008) Substructure system identification from coupled system test data. Mech Syst Signal Process 22(1):15–33

3. D'Ambrogio W, Fregolent A (2010) The role of interface DoFs in decoupling of substructures based on the dual domain decomposition. Mech Syst Signal Process 24(7):2035–2048. doi:10.1016/j.ymssp.2010.05.007. Also in Proceedings of ISMA 2010, Leuven, Belgium, pp 1863–1880
4. Sestieri A, Salvini P, D'Ambrogio W (1991) Reducing scatter from derived rotational data to determine the frequency response function of connected structures. Mech Syst Signal Process 5(1):25–44
5. Stanbridge A, Ewins D (1996) Measurement of translational and angular vibration using a scanning laser Doppler vibrometer. Shock Vib 3:141–152
6. Bello M, Sestieri A, D'Ambrogio W, La Gala F (2003) Development of PZT's as rotational transducers. Mech Syst Signal Process 17(5):1069–1081
7. Voormeeren SN, Rixen DJ (2012) A family of substructure decoupling techniques based on a dual assembly approach. Mech Syst Signal Process 27:379–396. doi:10.1016/j.ymssp.2011.07.028
8. D'Ambrogio W, Fregolent A (2011) Direct decoupling of substructures using primal and dual formulation. In: Conference proceedings of the Society of Experimental Mechanics series, vol 4. Linking models and experiments, vol 2, pp 47–76, Jacksonville, FL, 31 January–3 February, 2011. Springer, Berlin
9. D'Ambrogio W, Fregolent A (2012) Direct hybrid formulation for substructure decoupling. In: Conference proceedings of the Society for Experimental Mechanics series, vol 27. Topics in experimental dynamics substructuring and wind turbine dynamics, vol 2, pp 89–107, Jacksonville, FL, 30 January–2 February 2012